

Key Points:

- Several different radiometric systems provide common ages of approximately 4.3 Ga for the previously unstudied Apollo 16 Anorthosite Clast 60016,3A
- Lunar anorthosite Clast 60016,3A provides evidence for a basin-forming impact at approximately 4.3 Ga
- This has implications on the timing of the Late Accretion

Supporting Information:

- Supporting Information S1
- Table S1

Correspondence to:

N. E. Marks,
marks23@llnl.gov

Citation:

Marks, N. E., Borg, L. E., Shearer, C. K., & Cassata, W. S. (2019). Geochronology of an Apollo 16 clast provides evidence for a basin-forming impact 4.3 billion years ago. *Journal of Geophysical Research: Planets*, 124, 2465–2481. <https://doi.org/10.1029/2019JE005966>

Received 6 MAR 2019


Accepted 15 AUG 2019

Published online 3 OCT 2019

©2019. The Authors.

This is an open access article under the terms of the Creative Commons Attribution-NonCommercial License, which permits use, distribution and reproduction in any medium, provided the original work is properly cited and is not used for commercial purposes.

Geochronology of an Apollo 16 Clast Provides Evidence for a Basin-Forming Impact 4.3 Billion Years Ago

N. E. Marks¹ , L. E. Borg¹, C. K. Shearer², and W. S. Cassata¹

¹Nuclear and Chemical Sciences Division, Lawrence Livermore National Laboratory, Livermore, CA, USA, ²Institute of Meteoritics, University of New Mexico, Albuquerque, NM, USA

Abstract We examined lithic breccias from the Apollo sample collection in order to identify ferroan anorthosite samples suitable for geochronology, and better define the age relationships between rocks of the lunar highlands. Clast 3A is a previously unstudied noritic anorthosite from Apollo 16 lithic breccia 60016 with textural evidence of slow subsolidus recrystallization. We estimate a cooling rate of ~ 10 °C/Myr and calculate a pyroxene solvus temperature of 1,100–1,000 °C. Pyroxene exsolution lamellae (1–3 μm) indicate that the last stage of cooling was rapid at ~ 0.2 °C/year, typical of rates observed in thick ejecta blankets. We calculate concordant ages from the ^{147}Sm – ^{143}Nd , ^{146}Sm – ^{142}Nd , Rb–Sr, and Ar–Ar isotopic systems of $4,302 \pm 28$, $4,296 \pm 39$ – 53 , $4,275 \pm 38$, and $4,311 \pm 31$ Ma, respectively, with a weighted average of $4,304 \pm 12$ Ma. The closure temperature of the Sm–Nd system is $\sim 855 \pm 14$ °C, whereas the closure temperature of the Ar–Ar system is 275 ± 25 °C. Cooling from 855 to 275 °C at 10 °C/Myr should result in an age difference between the two isotopic systems of ~ 60 Myr. The concordant Sm–Nd, Rb–Sr, and Ar–Ar ages imply that they record the time the rock was excavated by a large impact from the midcrust. The ages clearly predate various late accretion scenarios in which an uptick in impacts at 3.8 Ga is preceded by a period of relative quiescence between 4.4 and ~ 4.1 Ga, and instead are consistent with decreasing accretion rates following the formation of the Moon.

Plain Language Summary We investigated a previously unexamined Apollo 16 ferroan anorthosite rock to study the timing of the formation of the lunar crust. Ferroan anorthosites are important because they are thought to be the oldest formed part of the lunar crust. Using three different isotopic geochronology methods, we determined that this rock (Clast 3A) is approximately 4.3 billion years old. The age is slightly younger than all but one recently dated ferroan anorthosite rock. The geology and textures of Clast 3A indicate that it formed deep within the lunar crust. The different dating methods record the age of the rock different temperatures. The Sm–Nd clock records the time when the rock cooled below about 855 °C, and the Ar–Ar clock records a temperature of about 275 °C. Identical ages determined from the two isotopic systems indicate that the rock experienced rapid cooling from above 855 °C to below about 275 °C. It appears that Clast 3A formed deep within the crust, but was then excavated 4.3 billion years ago by a massive cratering event. This implies that large basin forming impact events occurred on the Moon early in its history and not just around 3.8 billion years ago during the Late Heavy Bombardment.

1. Introduction

The lunar magma ocean (LMO) model describes the early differentiation of the Moon and predicts that rocks of the ferroan anorthosite suite (FAS) should be among the oldest lithologies. Chronologic investigations completed on these samples have yielded mixed results with ages spanning 283 Myr from 4,573 Ma (Alibert et al., 1994) to 4,290 Ma (Borg et al., 1999). The wide range of ages is problematic for two reasons. First, it implies that the LMO solidified very slowly, although numerical and thermal modeling predicts that it should, in fact, solidify within tens of million years if no surface conductive lid developed above the LMO (Elkins-Tanton et al., 2011; Herbert et al., 1977; Solomon & Longhi, 1977). A second difficulty is that the range of ages of the FAN lithologies perfectly overlaps the range of ages of Mg-suite rocks (Borg et al., 2015) that are thought to postdate anorthositic magmatism (Shearer et al., 2015; Shearer & Papike, 2005) because they contain the late stage LMO crystallization product rich in potassium (K), rare earth elements (REE), and phosphorous (P) known as urKREEP (Warren & Wasson, 1979). These inconsistencies are highlighted by a schematic timeline showing several important events in the history of lunar formation (Figure 1).

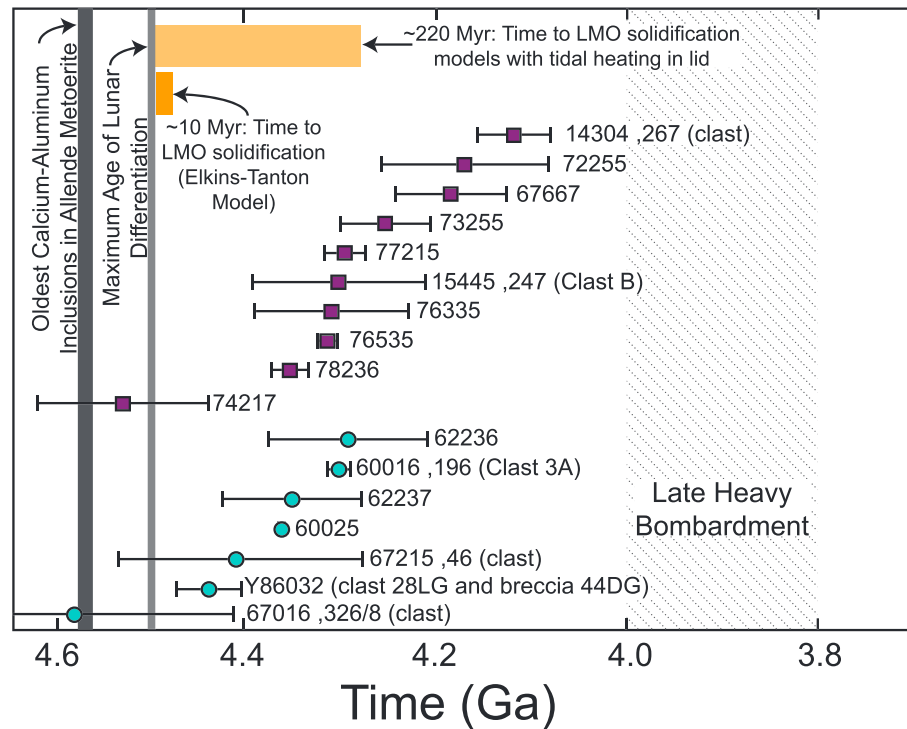


Figure 1. Timeline of ages relating the formation of the moon, lunar magma ocean (LMO) solidification, anorthositic crust formation, and late accretion events. The oldest calcium-aluminum rich inclusions in the Allende meteorite are depicted in the furthest left column based on the work of Connelly et al. (2008). The maximum age of lunar differentiation is based on the W isotope work that implies lunar differentiation occurred more than >70 Myr after solar system formation (Kruijjer & Kleine, 2017). LMO solidification models of Elkins-Tanton et al. (2011) as well as longer estimates (e.g., Meyer et al., 2010; Solomon & Longhi, 1977) are depicted at the maximum age of lunar differentiation; however, these estimates would shift to younger ages if lunar differentiation occurred later. Circles with error bars depict Ferroan Anorthosite Suite samples with reliable ages based on data from Borg et al. (2015), and references therein, Sio and Borg (2018), and this work. Squares with error bars depict Mg-Suite samples with reliable ages based on data included in Borg et al. (2015), and references therein. The schematic timing of the Late Heavy Bombardment is after Ryder (1990, 2002).

Ferroan anorthosite suite samples are difficult to date accurately, and this has probably contributed to the wide range in apparent ages reported. The FAS samples are nearly monomineralic, containing only small proportions of mafic minerals, have very low abundances of many elements used in chronologic investigations, and often have modified isotopic compositions resulting from the capture of thermal neutrons on the lunar surface. In addition, FAS samples are ancient, and have experienced metamorphism resulting from impacts thought to be associated with the Late Heavy Bombardment that mobilized most elements used for chronology. As a consequence, there are a very limited number of FAS samples that are large enough, have enough mafic minerals, and are metamorphosed minimally enough to be dated reliably. In fact, in the last ~30 years only a handful of FAS samples have yielded ages with low, geologically useful uncertainties (Figure 1; also see summary in Borg et al. (2015)). In addition, many lunar plutonic rocks cooled slowly enough that there are measurable differences between the time the rock was emplaced in the crust and the time when the chronometer closed (Borg et al., 2017; McCallum & Schwartz, 2001). To address these issues, and better constrain the age of ferroan anorthosite magmatism, we have searched lithic breccias in the Apollo 16 collection to identify additional samples that are suitable for chronologic investigations. Presented below are the results of a combined petrologic and chronologic investigation of noritic anorthosite Clast 3A from lithic breccia 60016. We find that this rock yields well defined, and concordant ages from multiple chronometric systems that do not record the crystallization age of the rock, but instead reflect the time when the sample was excavated from midcrustal depths.

2. Sample Selection and Processing

Sample 60016 was collected near the lunar module at the Apollo 16 landing site. It is an ancient fragmental polymict breccia, apparently formed during the period of basin formation (McKay et al., 1986; Ryder &

Norman, 1980). The sample is characterized by light and dark clasts set in a light grey matrix (Figure 2). The porous matrix is composed of crushed minerals and lithic fragments up to 2 mm in size, as well as glass spherules that range in size up to 1.5 mm. Several slabs and irregular pieces of 60016 were inspected to locate ferroan anorthosite clasts. Although most of the slabs lacked sufficiently large clasts to complete the detailed investigation necessary to both characterize and determine the age of the clast, a subsample of 60016, from slab 196, (60016,196) did have a sufficiently large clast. The clast was named 3A by Martinez (1985) and is pictured entrained in the breccia prior to extraction (Figure 2). It is described as a $15 \times 15 \times 20$ -mm clast of anorthosite containing approximately 30% light brown mafic minerals. We were allocated 3 g of Clast 3A and the remainder was removed from the slab and preserved separately in order to facilitate future investigations.

3. Methods

An abbreviated description of the analytical techniques used in this investigation is presented below. A more detailed description is presented in the supporting information along with mineral compositions and Ar isotope data.

3.1. Electron Probe Microanalysis

Thin section of Clast 3A, (,229), was characterized through backscattered electron imaging, X-ray mapping, and spot analyses of individual phases using the JEOL JXA-8200 Electron Probe Micro Analyzer at the University of New Mexico. Modal abundance of phases was directly determined from composite backscattered electron images of the entire clast via point counting. X-ray maps were collected under the following conditions: accelerating voltage of 15 kV and beam current of 50 nA. K_{α} X-ray maps for Ca, Cr, Fe, and Mg are presented in Figure 3. Quantitative Electron Probe Micro Analyzer point analyses were conducted under the following conditions: accelerating voltage of 15 kV, beam current of 20 nA, and spot size varying from 1 to 3 μm . The sample was repolished between the mapping campaign and the quantitative Electron Probe Micro Analyzer analyses. Standards for the point analyses consisted of a suite C.M. Taylor Company mineral and synthetic standards orthoclase (K,Al), olivine (Fe, Mg, Si), spessartine (Mn), rutile (Ti), anorthite (Ca), and albite (Na). Determination of the quality of the measurements was based upon totals being between 98 and 102% as well as on stoichiometric constraints for the phases being analyzed. Detection limits were calculated at the 3σ level. Representative mineral compositions are plotted in Figures 4 and 5 and presented in Table S1 in the supporting information.

3.2. Secondary Ion Mass Spectrometry

Our analytical approach followed Shearer et al. (2008, 2010). Trace element concentrations of individual phases were determined using the Cameca ims 4f, secondary ion mass spectrometry (SIMS) at the University of New Mexico. Measurements were made for La, Ce, Nd, Sm, Eu, Dy, Er, Yb, and Sr using the following analytical conditions: accelerating voltage 10 kV, voltage offset -75 V, and beam current 30 nA, resulting in a spot size ~ 20 – 30 μm . In cases where high spatial resolution was needed, the smaller field apertures were used. The ion probe analyses involved repeated cycles (10 cycles per analysis) of peak counting on the isotopes of select trace elements. Absolute trace element concentrations were calculated by normalizing to ^{30}Si . These normalized intensities were calibrated using the known concentration for laboratory pyroxene and plagioclase standards. The results are shown in Figure S1 and Table S2.

3.3. Noble Gas Analyses

Our analytical approach followed Cassata and Borg (2016). Noble gas extractions on Clast 3A were conducted in the Livermore Noble Gas Laboratory. Whole-rock fragments of Clast 3A were loaded into aluminum discs next to Fish Canyon sanidine neutron fluence monitors and irradiated for 50 hr at the Oregon State University TRIGA reactor. An ~ 1 -mg whole-rock fragment of 60016 was encapsulated in a small, high-purity, metal packet that was crimped at both ends. The packet was heated with a 75-W diode laser to extract Ar. The argon released in the heating steps was purified using four SAES getters, and analyzed using a Nu Instruments Noblesse mass spectrometer by peak hopping in the axial detector. Corrections were made for interfering nuclear reaction products (Renne et al., 2005), ^{37}Ar and ^{39}Ar decay, spectrometer discrimination, and extraction line blanks. Ages were calculated using the decay constants and standard calibration of Renne et al. (2011). The apparent cosmic ray exposure ages of each degassing step were

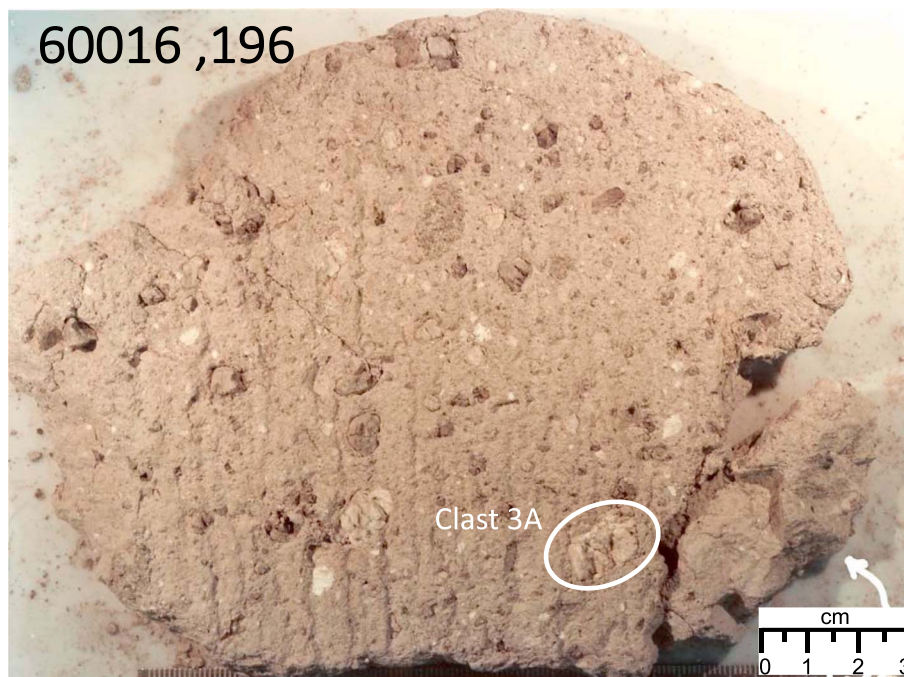


Figure 2. Photograph of lithic breccia slab 60016,196 (S84-41701). Clast 3A is the lighter grey clast within the oval.

calculated following the approach of Shuster and Cassata (2015), assuming a cosmogenic $^{38}\text{Ar}/^{36}\text{Ar}$ ratio of 1.54 (Wieler, 2002) and a trapped $^{38}\text{Ar}/^{36}\text{Ar}$ ratio of 0.19 (Levine et al., 2007). Uncertainties on Ar-Ar ages are quoted at 2σ throughout the paper and include uncertainty associated with decay constants.

3.4. Sample Digestion

A whole-rock fragment of Clast 3A was initially removed from the bulk sample for future analysis and the remainder was crushed in a synthetic sapphire mortar and pestle. The sample was then sieved using a stainless-steel sieve and nylon mesh yielding fractions of 75–200, 200–325, and <325 mesh. The size-sorted fractions were passed through a Frantz Magnetic Barrier Laboratory Separator and then hand-picked under dry conditions to achieve mineral separates (Figure S2). The <325 mesh powder, produced during sieving of the sample in preparation for mineral separations, is identified as the Fines fraction. The three mineral separates, Fines, and whole rock fractions were digested by standard techniques using hydrofluoric, nitric, and hydrochloric acids.

3.5. Bulk REE Analyses of Mineral Fractions

Small aliquots representing about 1% of the digested mineral fractions were analyzed for rare earth element concentrations using a Thermo XSI quadrupole Inductively Coupled Plasma Mass Spectrometer at Lawrence Livermore National Laboratory. The results are presented in Table S3 and Figure S1. External calibration was used to quantify elemental concentrations. Samples were diluted with 2% HNO_3 following digestion in order to achieve a 0.1% dissolved solid content prior to analysis. In order to correct for instrumental drift during the runs, an indium internal standard was added to all samples and standards, and instrument response was calibrated prior to and following the sample run using a six-point calibration curve that encompassed the range of concentrations in the samples.

3.6. Rb-Sr and Sm-Nd Analyses

Aliquots representing 5% of the total dissolved sample were spiked with ^{149}Sm and ^{150}Nd tracers; the remaining 95% fractions were spiked with ^{87}Rb and ^{84}Sr tracers. Rubidium, strontium, and REE were purified using Bio-Rad AG-50W-X8 cation exchange resin and 2M and 6M HCL elutions. Samarium and neodymium were separated in pressurized quartz columns with 0.2M α -HIBA acid. Samples analyzed for Nd isotope composition were passed through the α -HIBA columns twice to reduce ^{142}Ce interferences on ^{142}Nd which ranged from 12 to 24 ppm. Total procedural blanks were 17 pg Sm, 45 pg Nd, 9 pg Rb, and 24 pg Sr.

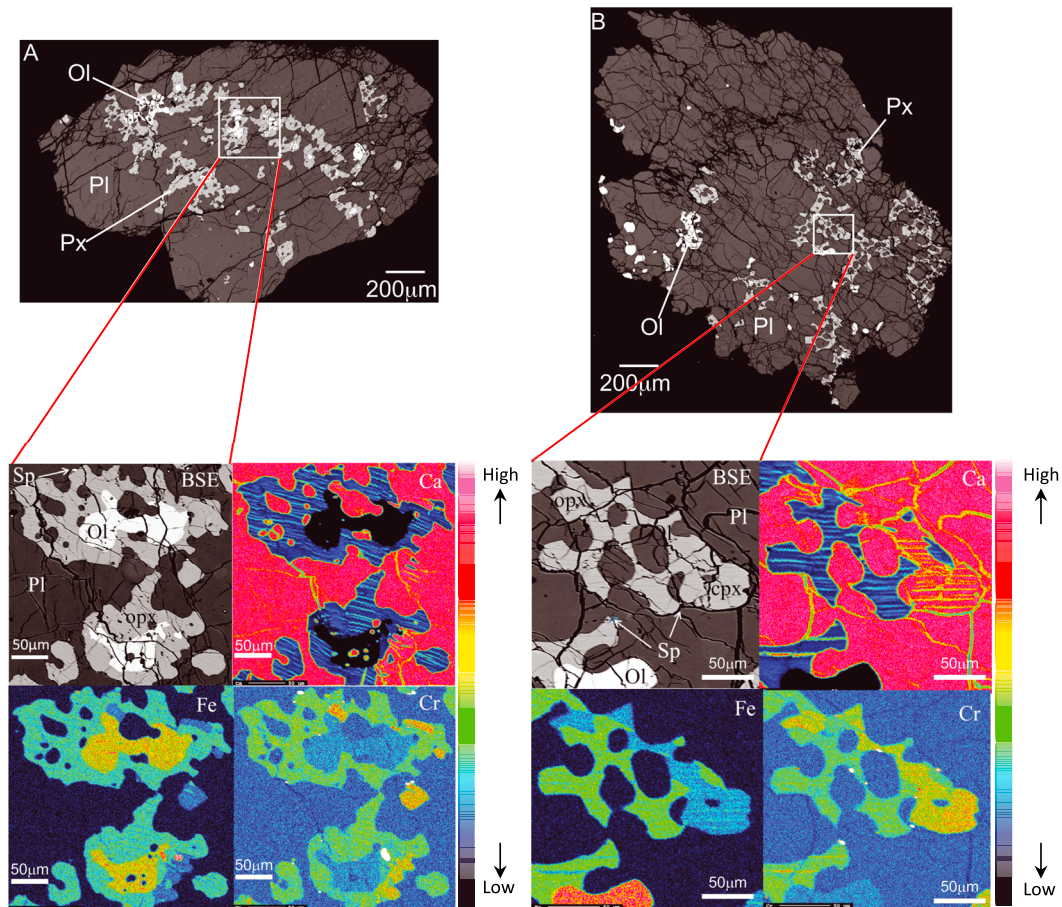


Figure 3. Backscatter electron image and trace element X-ray maps of 60016 Clast 3A. (a and b) Large BSE images from two chips of Clast 3A illustrating variable modal mineralogy of clast. Major minerals include plagioclase (Pl; dark grey), pyroxene (Px; light grey), and olivine (Ol; white); orthopyroxene (opx), clinopyroxene (cpx), and spinel (Sp) are also indicated. Insets are BSE and Ca, Fe, and Cr X-ray maps of selected areas of 60016 Clast 3A showing anhedral grains, poikiloblastic texture, and clinopyroxene exsolution lamellae. Exsolution lamellae are 1–3 μm in width. Color scale reflects the number of X-ray counts; that is, warm colors indicate higher concentration and cool colors indicate lower total concentration.

Isotope ratio measurements were made on a Thermo Scientific Triton thermal ionization mass spectrometer at Lawrence Livermore National Laboratory. Samarium was run a 0.8 to 1.5 V ^{149}Sm (10^{11} ohm amplifiers) for 200 ratios and corrected for internal mass fractionation using $^{147}\text{Sm}/^{152}\text{Sm} = 0.56083$. Neodymium was run in dynamic mode with ^{144}Nd beam intensities of 2.7–4.8 V for 510 to 1,080 ratios and corrected for mass fractionation using $^{146}\text{Nd}/^{144}\text{Nd} = 0.7219$. Average $^{142}\text{Nd}/^{144}\text{Nd}$ and $^{143}\text{Nd}/^{144}\text{Nd}$ ratios measured for the neodymium isotopic reference JNdi-1 (Tanaka et al., 2000) were 1.141837 ± 0.00005 and 0.512101 ± 0.000005 (2 standard deviation; $N = 7$). Strontium deposited on single zone refined Re filaments with a Ta_2O_5 emitter suspended in H_3PO_4 and run at an intensity of 2–5 V ^{88}Sr . Runs consisted of 200 cycles with 16.8s integration times. Mass fractionation was corrected using $^{86}\text{Sr}/^{88}\text{Sr} = 0.1194$. Replicate analyses of NBS-987 during the course of this study resulted in an external reproducibility corresponding to $^{87}\text{Sr}/^{86}\text{Sr} = 0.710249 \pm 0.000010$ (2 standard deviation; $N = 10$). Rubidium was loaded on single zone refined Re filaments with no emitter. Mass fractionation was corrected using NBS-984 using the measured $^{85}\text{Rb}/^{86}\text{Sr}$ of 2.603 ± 0.017 , assuming $^{85}\text{Rb}/^{86}\text{Sr}$ of NBS-984 of 2.953.

4. Results

4.1. Petrology and Geochemistry

Clast 3A contains 82.6% plagioclase, 15.2% of both low- and high-Ca pyroxene, 2.2% olivine, and a trace of chromite. It is therefore classified as a noritic ferroan anorthosite. The modal mineralogy measured from

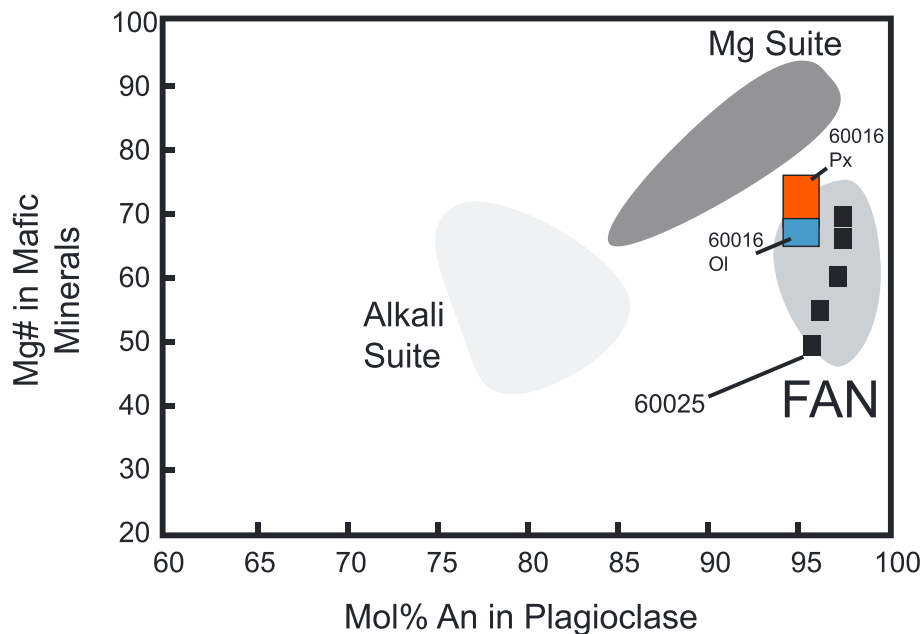


Figure 4. Plot of molar anorthosite content in plagioclase versus Mg# of pyroxene (red field) and olivine (Blue field) from Clast 3A. Mineral compositions from 60025 (dark squares) are plotted for comparison. Fields for Ferroan anorthosites (FAN), Mg-suite, and Alkali suite samples from Shearer et al. (2006). Although both 60016 and 60025 fall in the FAN field, 60025 has mafic phases with significantly more variable Mg#s.

the thin section is somewhat less mafic than the macroscopic description of the bulk clast described by Martinez (1985), suggesting that the clast may have a slightly heterogeneous distribution of mafic minerals. The clast has a coarse-grained plutonic texture, and is crosscut with pervasive microfractures that demonstrate minimal offset. Subhedral to anhedral plagioclase grains up to 1 mm in size best preserve the remnants of a coarse-grained plutonic texture. Pyroxene and olivine have a poikiloblastic-like texture and contain rounded inclusions of plagioclase that are 10–50 μm (Figure 3). The olivine is anhedral (50–150 μm) and partially to totally surrounded by anhedral pyroxene (100–400 μm) with an ameboid shape. Both low- and high-Ca pyroxenes exhibit fine-scale exsolution lamellae that are less than 3 μm wide (Figure 3).

4.1.1. Major-Minor Element Mineral Compositions

The composition of plagioclase and mafic silicates in Clast 3A plot within the field defined by ferroan anorthosites (Figure 4). All plagioclase grains exhibit a limited compositional range of $\text{An}_{96-94.5}$. The compositions of the high- and low-Ca pyroxenes is presented in the supporting information and plotted on Figure 4 along with pyroxene solvi at 1,100 and 800 $^{\circ}\text{C}$. Pyroxenes demonstrate limited variation in Mg content compared to the variation in Ca content and fall along a single tie-line. The Ca content of the low-Ca pyroxenes ranges from Wo_5 to Wo_{18} , and the Mg content ranges from En_{70} to En_{75} . The Ca content of the high-Ca pyroxenes ranges from Wo_{28} to Wo_{42} , whereas the Mg content ranges from En_{78} to En_{86} . The linear array on the pyroxene quadrilateral (Figure 5) is due to the inability of microprobe spots to spatially resolve exsolution exhibited by the two compositional types of pyroxenes. Bulk pyroxene compositions indicate subsolidus re-equilibration occurred between 1,100 and 1,000 $^{\circ}\text{C}$ based on calculations using the composition of high and low Ca pyroxenes from 60016 and the two pyroxene geothermometer of Lindsley and Andersen (1983). The data from Clast 3A are plotted along with pyroxene analyses from several grains in 60025 from James et al. (1991) for comparison purposes. Olivine also has a limited compositional range with Mg#s ranging from 65 to 67, CaO from 0.08 to 0.13 wt %, MnO from 0.29 to 0.34 wt %, and Cr_2O_3 from 0.03 to 0.06 wt %.

4.1.2. Rare Earth Element Compositions of Minerals

The trace element compositions of minerals were determined from both bulk analysis of mineral fractions and SIMS analyses of phases in thin section and are presented in the supporting information. There is excellent agreement between the rare earth element abundances determined in plagioclase by both techniques indicating that the plagioclase mineral fractions are relatively pure. Plagioclase demonstrates a slightly

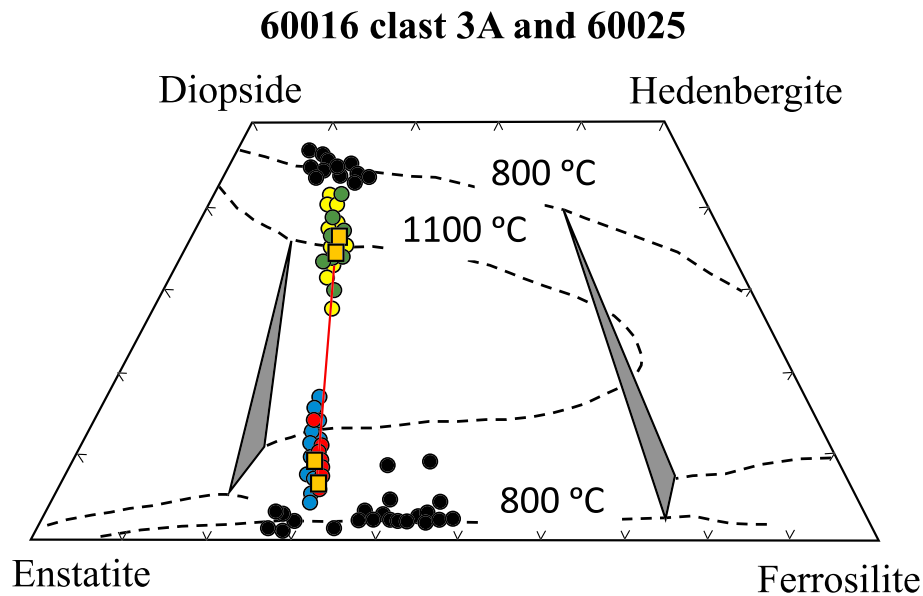


Figure 5. Pyroxene quadrilateral illustrating compositional variation in pyroxenes from FAS clast 60016 and “bulk” pyroxene compositions plotted with pyroxene solvi at 1,100 and 800 °C. Colored symbols are analyses of spots from individual pyroxene grains in 60016. Filled black symbols pyroxene analyses from several grains in 60025 from James et al. (1991). Note wide compositional range in 60025 compared to 60016. Bulk composition of high- and low-Ca pyroxenes from 60016 represented by orange squares are used to calculate the temperature of pyroxene subsolidus growth between 1,000 and 1,100° using two pyroxene geothermometer of Lindsley and Andersen (1983).

light rare earth element (LREE) enriched pattern with a large positive Eu anomaly that is typical of plagioclase compositions measured in other FAS samples. The compositions of pyroxenes determined by SIMS have a more LREE-depleted pattern in comparison to the mineral fractions. In addition, the SIMS data for pyroxene are characterized by negative Eu anomalies, whereas the mineral fractions are characterized by positive ones, suggesting that the pyroxene mineral fractions contain small amounts of plagioclase. Like the plagioclase, the REE data obtained by SIMS on pyroxenes are typical of other FAS samples (Papike et al., 1997, 1998).

4.2. Ar Chronology

A bulk fraction of Clast 3A yields a concordant age spectrum with a plateau age containing >95% of the gas released of $4,311 \pm 31$ Ma (Figure 6a). Discordance observed over the last 5% of the ^{39}Ar released is associated with pyroxene- and olivine-derived gas, as indicated by the variable Ca/K ratios (Figure 6c) compared to the preceding plagioclase-derived gas extractions. This may reflect subtle recoil redistribution of ^{39}Ar into smaller (tens of microns), poikilitic mafic minerals (Figure 3). Clast 3A also yields a concordant exposure age spectrum with a $^{38}\text{Ar}_{\text{cos}}/^{37}\text{Ar}$ plateau age containing >95% of the gas released of 1.13 ± 0.06 Ma. The exposure age is roughly consistent with excavation from South Ray Crater, which is estimated to be ~ 2 Ma (Arvidson et al., 1975).

4.3. Sm-Nd Chronology

In order to assess the effects of secondary neutron capture on the Sm-Nd systematics of Clast 3A, the isotopic composition of Sm was measured on an unspiked whole-rock fraction. The ^{149}Sm isotope has a very large thermal neutron capture cross section making it an excellent dosimeter. Neutron capture is therefore manifest by depletions of ^{149}Sm and excesses of ^{150}Sm relative to terrestrial standards. The measured Sm isotopic composition of 60016 demonstrated minimal evidence for neutron capture having an $\epsilon^{149}\text{Sm} = -0.89 \pm 0.10$ and $\epsilon^{150}\text{Sm} = +1.67 \pm 0.12$, consistent with the very young Ar exposure age. The shift in Sm isotopic compositions were so small that corrections made to $^{147}\text{Sm}/^{144}\text{Nd}$, $^{143}\text{Nd}/^{144}\text{Nd}$, and $^{142}\text{Nd}/^{144}\text{Nd}$ isotopic ratios had no effect on the slopes or intercepts of the Sm-Nd isochrons.

Samarium-neodymium data are presented in Table 1. A ^{147}Sm - ^{143}Nd isochron with an age of $4,302 \pm 28$ Ma, and an initial $\epsilon^{143}\text{Nd} = -0.28 \pm 0.14$ (Figure 7a), is calculated using the Isoplot v4.1 program of Ludwig

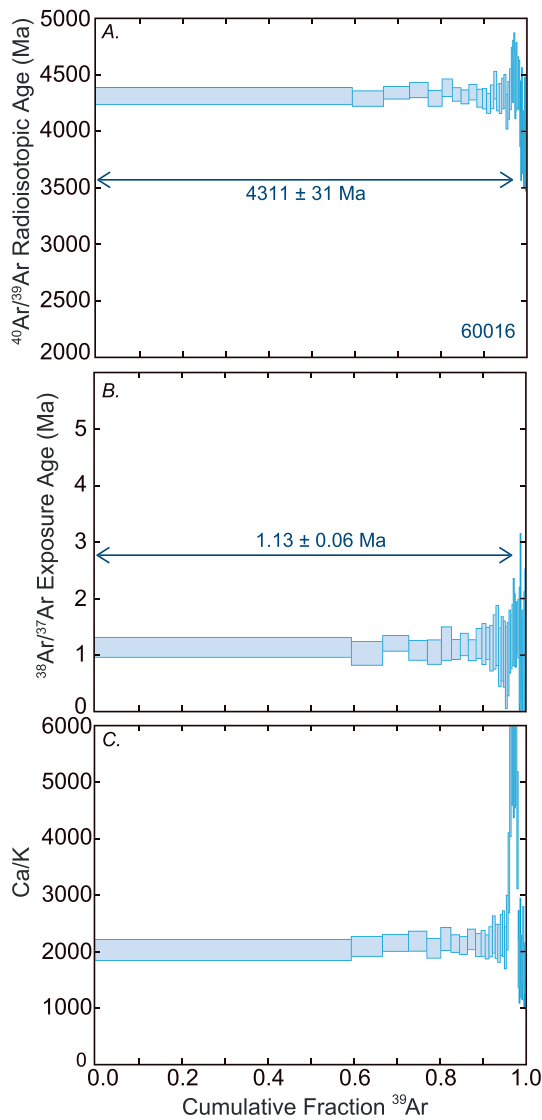


Figure 6. (a) Apparent $^{40}\text{Ar}/^{39}\text{Ar}$ radioisotopic age, (b) $^{38}\text{Ar}/^{37}\text{Ar}$ cosmogenic age, and (c) Ca/K spectra for sample 60016. The cumulative release fraction of ^{39}Ar released is plotted against each spectrum. Vertical dimensions of boxes reflect $\pm 2\sigma$ analytical uncertainties.

(1991). Note that all of the analyzed mineral fractions and whole rocks lie on the 4,302-Ma isochron (Figure 7a inset), implying that all of the mineral phases are in isotopic equilibrium. This is confirmed by the small mean square weighted deviation (MSWD) of 2.0 determined for the regression. The initial $\epsilon^{143}\text{Nd}$ value calculated from the regression indicates that Clast 3A was derived from a source that had a chondritic, to very slightly LREE enriched, REE pattern. Petrogenetic modeling of LMO solidification predicts that plagioclase-rich floatation cumulates will be derived from such sources (Snyder et al., 1992; Shearer et al., 2006, 2015), lending confidence that the Sm-Nd age is not recording a postcrystallization event associated with impact metamorphism.

A ^{147}Sm - ^{142}Nd isochron is presented in Figure 7b in which the slope of the regression corresponds to the $^{146}\text{Sm}/^{144}\text{Sm}$ ratio of the rock at the time it formed. A model age is determined by calculating the time it takes for the $^{146}\text{Sm}/^{144}\text{Sm}$ ratio, inherited by the rock when it formed, to decay from the solar system initial value at 4,567 Ma of 0.00828 ± 0.00044 (Marks et al., 2014) using the ^{146}Sm half-life of 103 Myr determined by Meissner et al. (1987). In the case of Clast 3A, the slope of the regression corresponds to an age of $4,296 \pm 39/-53$ Ma (Figure 7b). The age is defined by all five mineral separates and whole rocks and has a very low MSWD of 0.35 indicating a good fit of the data to the regression. The young age of the rock is supported by the observation that $^{142}\text{Nd}/^{144}\text{Nd}$ ratios of the mineral fractions vary by only 22 ppm, indicating that ^{146}Sm was almost extinct at the time this sample cooled below the closure temperature of the Sm-Nd system. The initial $\epsilon^{142}\text{Nd}$ value of -0.14 ± 0.05 determined from the $^{147}\text{Sm}/^{144}\text{Nd}$ - $^{142}\text{Nd}/^{144}\text{Nd}$ regression (Figure 7b) is consistent with derivation from a source with an initial $^{142}\text{Nd}/^{144}\text{Nd}$ slightly lower than that inferred for the Earth assuming a chondritic $^{147}\text{Sm}/^{144}\text{Nd}$ ratio of 0.1967. This observation again supports the contention that the rock cooled below the blocking temperature of the Sm-Nd system ~ 4.3 Ga.

4.4. Rb-Sr Chronology

Rubidium-strontium data are presented in Table 2. Unfortunately, there is not sufficient spread in the $^{87}\text{Rb}/^{86}\text{Sr}$ ratios to obtain an isochron age. Instead, all of the mineral and whole-rock fractions have nearly identical $^{87}\text{Rb}/^{86}\text{Sr}$ and $^{87}\text{Sr}/^{86}\text{Sr}$ ratios. An initial $^{87}\text{Sr}/^{86}\text{Sr}$ ratio of Clast 3A of 0.699062 ± 11 is calculated from all of the fractions using the Sm-Nd age of 4,302 Ma. This corresponds to a Best Achondrite Basalt Initial model age of $4,275 \pm 38$ Ma, calculated assuming the solar system initial

$^{87}\text{Sr}/^{86}\text{Sr}$ value of 0.69898 and a bulk Moon $^{87}\text{Rb}/^{86}\text{Sr}$ of 0.020 ± 0.006 (1 standard deviation) derived from the average estimates of Anders et al. (1977), Taylor (1982), and Wänke et al. (1977). The age uncertainty is determined from 2 times the standard deviation of Best Achondrite Basalt Initial model ages calculated for each mineral fraction. The agreement between the Best Achondrite Basalt Initial model Rb-Sr age, the Ar-Ar, and Sm-Nd ages suggests that the ages record when the sample cooled quickly below the closure temperatures of the various chronometers. The best estimate for this event is $4,304 \pm 12$ Ma (MSWD = 1.08) represented by the weighted average of all of the measured ages.

5. Discussion

5.1. Age Relationships of Lunar Rocks

The abundance, widespread distribution, Ca and Fe-rich mineral compositions, bulk rock compositional characteristics, and apparent antiquity of the ferroan anorthosites have led to the suggestion that FAS samples are ancient floatation cumulates from the LMO (e.g., Wood et al., 1970). However, recent age

Table 1
Sm-Nd Isotopic Data From 60016 Clast 3A

Fraction	Wt (mg)	Sm (ppm) ^a	Nd (ppm) ^a	$\frac{^{147}\text{Sm}_{\text{a,d}}}{^{144}\text{Nd}}$	$\frac{^{143}\text{Nd}_{\text{b}}}{^{144}\text{Nd}}$	$\frac{^{142}\text{Nd}_{\text{b}}}{^{144}\text{Nd}}$
Plag I	957.0	0.152	0.598	0.15334 ± 15	0.511399 ± 2	1.141808 ± 4
Plag II	342.7	0.152	0.597	0.15345 ± 15	0.511389 ± 7	1.141805 ± 13
Px	182.2	0.243	0.659	0.22249 ± 22	0.513362 ± 3	1.141827 ± 9
Wr	213.1	0.162	0.633	0.1551 ± 16	0.511431 ± 4	1.141812 ± 9
Fines	147.6	0.190	0.690	0.16656 ± 17	0.511765 ± 5	1.141815 ± 12
JNdi Nd Std 500 ng (N = 8)					0.512003 ± 10 ^c	1.141839 ± 7

Note. Samples and standards were run as Nd⁺.

^aThe reported uncertainties apply to last digits and include a minimum uncertainty of 0.5%, plus 50% of the blank correction for Sm and Nd added quadratically. ^bNormalized to $^{146}\text{Nd}/^{144}\text{Nd} = 0.7219$. The reported uncertainties apply to last digits and are $2\sigma_{\text{m}}$ (2 times the standard error of measured isotopic ratios). ^cThe uncertainties refer to last digits and are $2\sigma_{\text{p}}$ (2 times the standard deviation of population of mass spectrometry runs on isotopic standard). The isochrons are calculated using the larger uncertainty, either $2\sigma_{\text{p}}$ (from standard runs) or $2\sigma_{\text{m}}$ (from measured isotopic ratios). ^dThe $^{147}\text{Sm}/^{144}\text{Nd}$ corrected for neutron capture using Sm isotopic composition measured on an unspiked whole rock fraction. Sm isotopic composition is $\epsilon^{149}\text{Sm} = -0.89 \pm 0.10$ and $\epsilon^{150}\text{Sm} = +1.67 \pm 0.12$.

determinations suggest that they are not particularly old and that the young age of Clast 3A is not unique. Ages of $4,359 \pm 3$, $4,294 \pm 58$, and $4,359 \pm 65$ Ma were calculated for ferroan noritic anorthosites 60025 (Borg et al., 2011) and 62236 (Borg et al., 1999), as well as ferroan troctolitic anorthosite 62237 (Sio & Borg, 2018), respectively. Some of the oldest FAS samples, such as 67016 ($4,573 \pm 160$ Ma; Alibert et al., 1994) and 67215 ($4,408 \pm 130$ Ma; Norman et al., 2003), have large uncertainties and MSWDs in excess of 6 (Borg et al., 2015). Other old FAS ages, such as the $4,437 \pm 39$ -Ma age determined on 60025 by Carlson and Lugmair (1988), have not been repeated by more recent studies (Borg et al., 2011). The young ages of FAS samples are also concordant with ages determined on other lunar lithologies argued to represent primordial solidification products of the LMO. This includes urKREEP model ages of $4,353 \pm 37$ and $4,389 \pm 45$ Ma (Gaffney & Borg, 2014) and average mare basalt source region age of $4,337 \pm 24$ Ma (Brandon et al., 2009; Borg et al., 2019; Boyet & Carlson, 2007; McLeod et al., 2014; Nyquist et al., 1995; Rankenburg et al., 2006; also see summary in Borg et al., 2015).

The 4.30- to 4.36-Ga ages are also observed in lithologies thought to represent secondary magmatism intruded into the anorthositic crust. Some examples that have been recently dated include Mg-suite troctolite 76535 ($4,306 \pm 10$ Ma; Borg et al., 2017), as well as Mg-suite norites 78286 ($4,349 \pm 19$ Ma; Edmunson et al., 2009) and 77215 ($4,288 \pm 22$ Ma; Carlson et al., 2014). In addition, there is a clear peak in ages of zircon derived from the Alkali-suite rocks at 4,340 Ma (Borg et al., 2015; Nemchin et al., 2008). This implies that widespread magmatism was occurring on the Moon around 4.35 Ga and that it involved rocks present in the mantle (mare basalt sources and urKREEP), as well as in the crust (Mg, Alkali, and Ferroan Anorthosite suites).

5.2. Thermal History of 60016 Clast 3A and 60025

5.2.1. Geologic Significance of Clast 3A Ages

Some of the variation in ages determined for lunar plutonic rocks is likely to reflect their different cooling histories (McCallum & Schwartz, 2001), so that the significance of an individual age must be viewed in this context. A cartoon illustrating the potential cooling history of Clast 3A is shown in Figure 8. Initially, the parental magma containing plagioclase, olivine, and minor amount of pyroxene solidifies in the crust. Elkins-Tanton et al. (2011) estimated that plagioclase crystallization and flotation in the LMO started at $\sim 1,100$ °C, whereas Ford et al. (1977) estimated the anhydrous solidus of anorthositic magmas to be $\sim 1,200$ °C. Hess and Parmentier (1995) and Van Orman and Grove (2000) determined that LMO reached ilmenite saturation between 1,180 and 1,125 °C, suggesting that plagioclase saturation, occurring slightly earlier, would be around 1,200 to 1,150 °C (Snyder et al., 1992). The first minerals to crystallize were initially zoned, becoming progressively more Na (plagioclase) and Fe (pyroxene and olivine) rich toward the rims. However, slow cooling in the crust homogenized these phases and produced the poikiloblastic texture observed in the clast (Figure 3). The lack of coarse pyroxene exsolution lamellae indicates that the temperature remained near the top of the pyroxene solvus. The period of slow cooling was followed by a period of

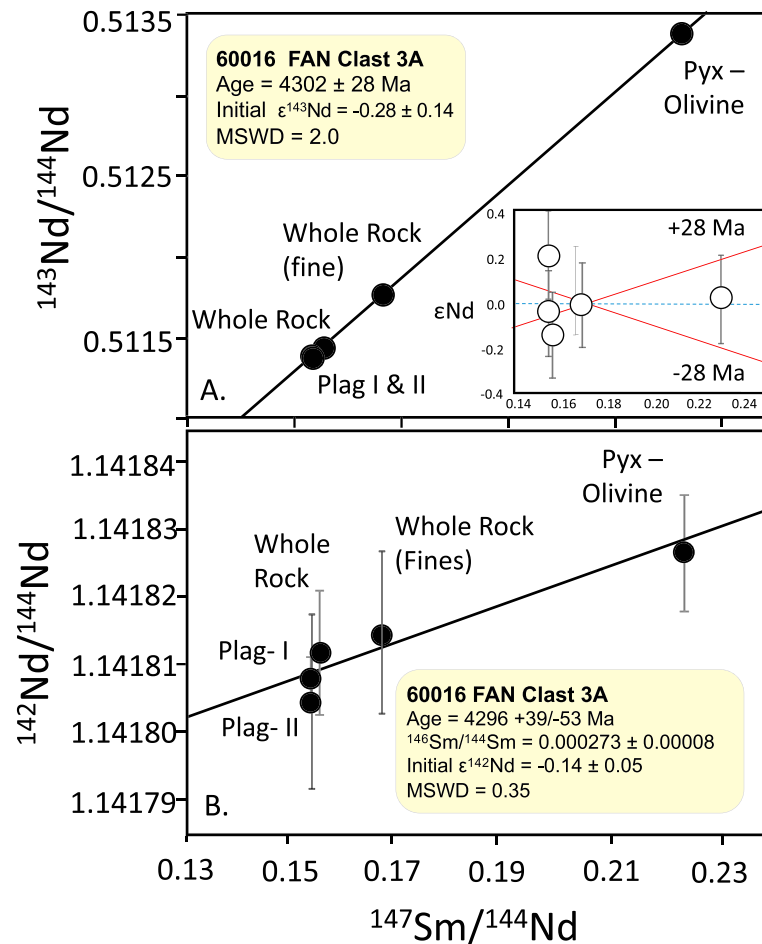


Figure 7. Sm-Nd isotopic plots of mineral fractions from Clast 3A. (a) The ^{147}Sm - ^{143}Nd plot yielding an age of $4,302 \pm 28$ Ma. (b) The ^{146}Sm - ^{142}Nd plot yielding a slope of 0.000273 ± 0.00008 . An age of $4,296 + 39/-53$ is calculated from the slope based on the initial $^{146}\text{Sm}/^{144}\text{Sm}$ of 0.00828 ± 0.00044 determined by Marks et al. (2014) and the 103-Ma half-life.

more rapid cooling implied by extremely fine 1–3- μm exsolution lamellae in the pyroxenes. McCallum and O'Brien (1996) demonstrated that the thickness of lamellae could be used to estimate the cooling rate of a sample. Their calibration suggests that the last stage of cooling was at a rate of 0.2 $^{\circ}\text{C}/\text{year}$. This cooling rate contrasts with the slow cooling rate implied by the texture and composition of minerals in Clast 3A, most likely reflecting rapid cooling in an ejecta blanket after excavation from the deep crust.

Temperatures that pyroxene last equilibrated in the crust have been estimated from the bulk compositions of coexisting low- and high-Ca pyroxenes (paired pyroxene compositions prior to exsolution) and indicate that homogenization and growth of the minerals in Clast 3A occurred around 1,100 to 1,000 $^{\circ}\text{C}$ (Figure 5). This temperature overlaps with estimated temperatures of the crest of the pyroxene solvus (e.g. Bohlen & Essene, 1978, Lindsley, 1983, Ross et al., 1973, Ross & Huebner, 1975). The pyroxene equilibrium temperature at depth is well above the temperature at which the Sm-Nd system is closed with respect to diffusive re-equilibration. For example, closure temperatures for 1-mm-radius anorthite grains with spherical geometry calculated using the equations of Ganguly and Tirone (1999), the diffusion parameters obtained by Cherniak (2003), and assuming cooling rates of 1, 10, and 100 $^{\circ}\text{C}/\text{Myr}$ are 799 ± 16 $^{\circ}\text{C}$, 855 ± 14 $^{\circ}\text{C}$, and 919 ± 12 $^{\circ}\text{C}$, respectively (errors reflect uncertainties associated with the experimentally determined diffusion parameters). Pyroxene closure temperatures calculated using the diffusion parameters of Cherniak and Liang (2007) are similar, and estimated to be $768 + 70/-104$ $^{\circ}\text{C}$, $836 + 61/-99$ $^{\circ}\text{C}$, and $907 + 54/-86$ $^{\circ}\text{C}$, respectively. This implies that the Sm-Nd isotopic system did not close when the sample was at depth.

Table 2
Rb-Sr Isotopic Data From 60016 Clast 3A

Fraction	Wt (mg)	Rb (ppm)	Sr (ppm)	$\frac{^{87}\text{Rb}}{^{86}\text{Sr}}$	$\frac{^{87}\text{Sr}}{^{86}\text{Sr}}$
Plag I	14.92	0.0580	183.1	0.00092 ± 1	0.699117 ± 5
Plag II	17.21	0.0643	208.8	0.00089 ± 1	0.699120 ± 5
Px	182.2	0.0442	131.4	0.00097 ± 1	0.699115 ± 6
Wr	10.79	0.0692	217.5	0.00092 ± 1	0.699124 ± 5
Fines	9.25	0.0668	185.7	0.00104 ± 1	0.699116 ± 5
NBS-987 500 ng (N = 10)					0.710249 ± 10 ^c

Note. The long-term $^{85}\text{Rb}/^{87}\text{Rb}$ ratio measured on more than 30 runs of NBS-984 Rb standard was 2.603 ± 17 ($2\sigma_p$) and was used to correct for instrument mass fractionation.

^aThe reported uncertainties apply to last digits and include a minimum uncertainty of 1% plus 50% of the blank correction for Rb and Sr, added quadratically. ^bNormalized to $^{86}\text{Sr}/^{88}\text{Sr} = 0.1194$. Reported uncertainties refer to last digits and are $2\sigma_m$ (2 times the standard error of measured isotopic ratios). ^cUncertainties refer to last digits and are $2\sigma_p$ (2 times the standard deviation of the population of analyses on the isotopic standard). Isochrons are calculated using either $2\sigma_p$ (from standard runs) or $2\sigma_m$ (from measured isotopic ratios), whichever is larger.

A better estimate of the closure temperature of the Sm-Nd system is obtained from tighter constraints on the cooling rate of Clast 3A derived by comparing its texture to the textures of other samples with well-defined cooling rates. The cooling rate of troctolite 76535 is estimated to be 1–5 °C/Myr (Nord, 1976; Stewart, 1975). This sample has a symplectite texture and contains minerals that are completely homogeneous meeting at 120° angles, indicating that this is one of the slowest cooled lunar samples (Elardo et al., 2012). The absence of symplectite textures and 120° triple junctions implies that Clast 3A cooled in excess of 1–5 °C/Myr. In contrast, sample 60025 has been estimated to have cooled at 18 °C/Myr (McCallum & O'Brien, 1996), consistent with the presence of compositionally heterogeneous mineral phases. As a consequence, Clast 3A is estimated to have cooled at an intermediate rate of ~10 °C/Myr, which corresponds to a closure temperature for the Sm-Nd system of 855 ± 14 °C.

If Clast 3A was exhumed from depth when it was at the pyroxene solvus temperature of 1,100 to 1,000 °C, and the Sm-Nd isotopic system closed in this sample at 855 ± 14 °C, then the $4,302 \pm 28$ -Ma Sm-Nd age must record the time at which the sample was excavated from depth. Thus, the Sm-Nd age of Clast 3A records the time when the sample underwent rapid cooling recorded by the thin exsolution lamellae. The $^{40}\text{Ar}/^{39}\text{Ar}$

age of $4,311 \pm 31$ Ma determined for the sample supports this interpretation. The closure temperature for ^{40}Ar in ~1-mm-sized anorthite, like that in Clast 3A, is $\sim 275 \pm 25$ °C (Cassata & Renne, 2013), which is well below the equilibrium temperature calculated for the pyroxenes. Excavation followed by quick cooling at a rate near 0.2 °C/year near the lunar surface would quench both isotopic systems and result in the observed concordance between the Sm-Nd and Ar-Ar ages. On the other hand, if Clast 3A cooled very slowly through the Sm-Nd and Ar-Ar closure temperatures at depth, the pyroxene miscibility gap would be larger, the pyroxenes would fall near the 800 °C isotherm on Figure 4, thick exsolution lamellae would be obvious, and the Sm-Nd age would be ~60 Myr older than the Ar-Ar age. The weighted average age of $4,304 \pm 12$ Ma obtained from analysis of Clast 3A is therefore interpreted to record the time when the sample was excavated from depth.

5.2.2. Temporal Relationship Between FAS Samples

Ferroan anorthosite suite sample 60025 is another well-dated FAS sample that has had a very different cooling history than Clast 3A (Figure 9). Below we explore whether the ~60-Myr difference in the measured ages of 60025 and Clast 3A reflects differences in their respective cooling histories, or an extended period of FAS magmatism. This discussion is based on chronologic investigations completed by Borg et al. (2011) and the cooling history for 60025 outlined by McCallum and O'Brien (1996). The petrologic effects of cooling of 60025 are depicted in Figure 7. Like Clast 3A, the parental magma of 60025 initially crystallized plagioclase, pyroxene, and olivine. Although the modal proportions of olivine and pyroxene in 60025 and Clast 3A differ, the mineral chemistry is similar. Initially, both suites of minerals were compositionally zoned. McCallum and O'Brien (1996) estimated that 60025 cooled at a rate of 18 °C/Myr from 1,100 °C to 800 °C and from this they calculated a depth of emplacement of 21 km. Cooling at a moderate rate resulted in partial homogenization of the pyroxene and olivine grains and exsolution of clinopyroxene from low-Ca pyroxene producing thick exsolution lamellae that are ~40 μm in width. The final stage of cooling likely occurred in the upper crust where a secondary set of fine exsolution lamellae were produced (Hodges & Kushiro, 1973), and where the sample was heavily brecciated (McCallum & O'Brien, 1996).

The Ar-Ar age of 60025 is $4,272 \pm 39$ Ma (recalculated from Fernandes et al. (2013) using the decay constant and standard calibration of Renne et al. (2011)) and is concordant with the Ar-Ar age determined for 60016 Clast 3A of $4,311 \pm 31$ Ma. Samples 60025 and Clast 3A also yield similarly young cosmic ray exposure ages of 2.1 ± 0.3 Ma (Fernandes et al., 2013) and 1.13 ± 0.06 Ma, respectively, when calculated using a nominal surface production rate without detailed corrections for shielding. Excavation of both samples around 4.30 Ga followed by emplacement in similar locations in the ejecta blanket is consistent with the similarity of the exposure and Ar-Ar ages, their similar sampling locations on the Moon, and the occurrence of thin exsolution lamellae indicative of rapid cooling near the surface.

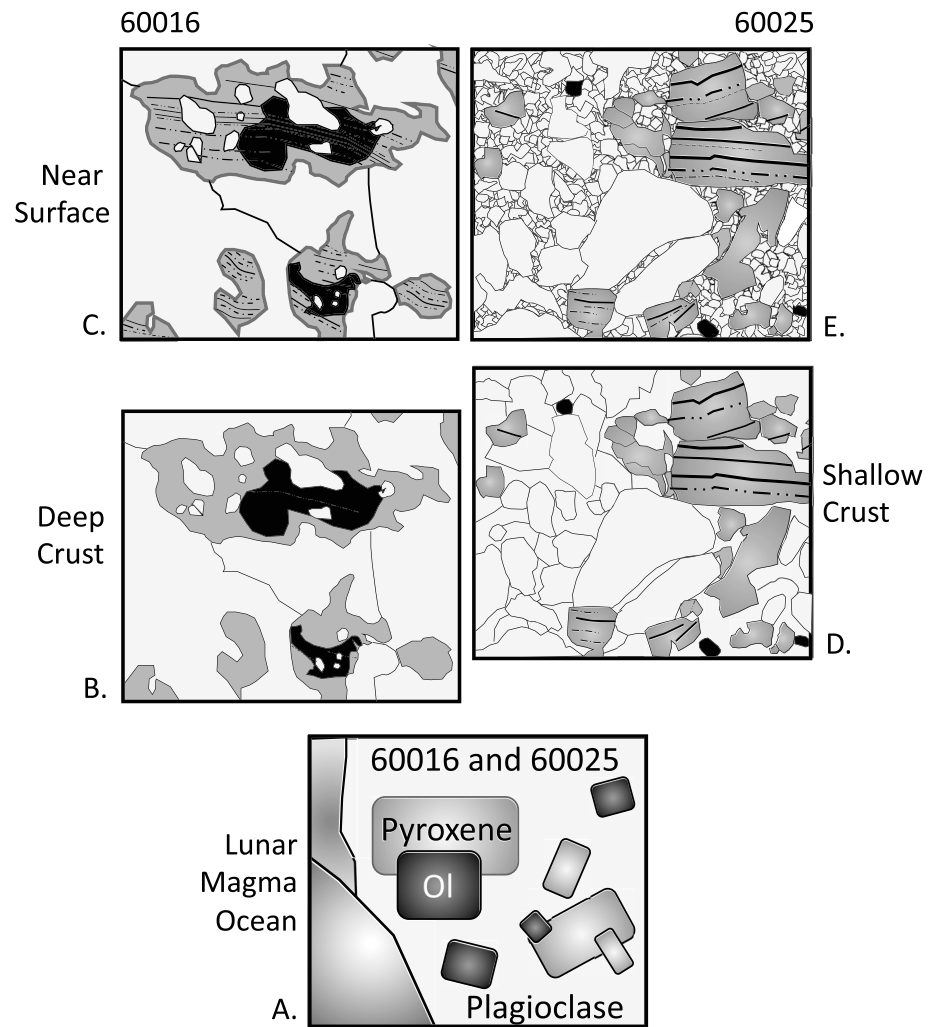


Figure 8. Cartoons depicting proposed cooling history of FAS samples 60016 Clast 3A and 60025. (a) Crystallization and flotation from LMO. (b and c) Cooling history of 60016 and (d and e) cooling of 60025. (b) Pyroxene + olivine growth and NaSi-CaAl diffusion in plagioclase and Fe-Mg diffusion in mafic minerals between 1,000 and 1,100 °C with cooling rate estimated to be 10 °C/Myr. (c) Fine-scale pyroxene exsolution in shallow crust during rapid cooling from ~850 °C. The rapid cooling rate estimated from pyroxene lamellae of 0.2 °C/year corresponds to a depth of >0.5 km. (d) Development of coarse-scale pyroxene exsolution and NaSi-CaAl diffusion in plagioclase at ~21 km between 1,050 and 800 °C. The cooling rate estimated for 60025 is estimated to be 18 °C/Myr by McCallum and Schwartz (2001). (e) Brecciation and minor addition to exsolution in shallow crust during rapid cooling from 800 °C. Final cooling that occurs at a rate 0.2 °C/year corresponds to a depth <0.5 km.

Sample 60025 has a Sm-Nd isochron age of $4,367 \pm 11$ -Ma age (Borg et al., 2011) that records the age when 60025 was at ~870 °C in the crust (Borg et al., 2017). The observation that the Sm-Nd age of 60025 is ~95 Myr older than the Ar-Ar age requires 60025 to have cooled below the 870 °C closure temperature prior to excavation. Thus, the ~65-Myr difference between the Sm-Nd ages of 60025 ($4,367 \pm 11$ Ma) and Clast 3A ($4,302 \pm 28$ Ma) is likely to reflect more rapid cooling of 60025. In this case, Clast 3A was intruded in the lunar crust at about the same time as 60025, but at a greater depth. Clast 3A cooled more slowly than 60025, and was above the closure temperature of both the Sm-Nd and Ar-Ar isotopic systems when it was excavated to the lunar surface (Figure 8).

5.3. An Impact at ~4,310 Ma Recorded by 60025 and 60016

Pre-Nectarian ejecta are thought to comprise a substantial quantity of Apollo 16 regolith (Haskin et al., 2002; Petro & Pieters, 2006), particularly in the Cayley formation. Both Clast 3A and 60025 represent plutonic

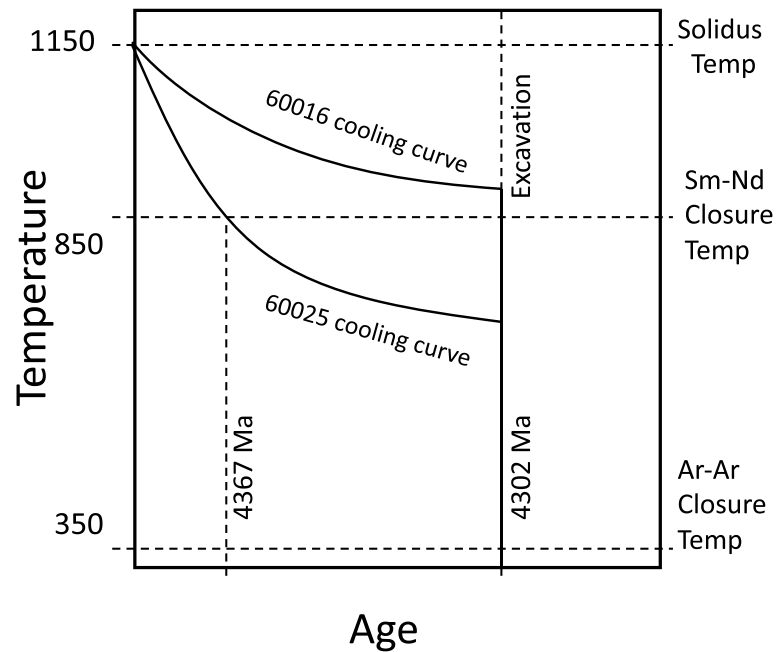


Figure 9. Schematic depicting proposed cooling history of FAS samples 60016 Clast 3A and 60025. Both samples are emplaced near their solidus temperature of $\sim 1,150$ °C but cool at different rates according to emplacement depth in crust. 60025 cools past the closure temperature of Sm-Nd and Pb-Pb of ~ 850 °C at depth, recording ages of $\sim 4,367$ Ma. 60016 cools more slowly. The Sm-Nd closure temperature is not reached when the sample is at depth. Instead excavation occurs near 4,310 Ma, when both samples are exhumed from the deep crust and cooled quickly near the lunar surface. At this time the Ar-Ar system closes recording the exhumation event.

rocks from the Cayley formation and provide evidence for a basin-forming impact at $4,304 \pm 12$ Ma. The Ar-Ar plateau ages of Clast 3A and 60025 of $4,311 \pm 31$ and $4,272 \pm 39$ Ma, respectively, are indistinguishable from Ar-Ar ages of anorthosites collected at the Luna 20 site (Cadogan & Turner, 1977; Cohen et al., 2001) and glass from the Luna 16 site (Cohen et al., 2001). As noted above, 60025 formed at ~ 21 -km depth in the crust (McCallum & O'Brien, 1996), and was excavated by an event defined by its Ar-Ar age, as well as the Ar-Ar and Sm-Nd ages of Clast 3A. The inferred crater diameter associated with excavation from 21-km depth is ~ 370 km, assuming that the excavation depth is 1/10th the diameter of the transient impact cavity, and the ratio of observed crater rim diameter to transient cavity diameter is ~ 1.75 (Garrick-Bethell et al., 2008; Wiczorek & Phillips, 1999). Clast 3A yields concordant Sm-Nd and $^{40}\text{Ar}/^{39}\text{Ar}$ ages, consistent with excavation from an even greater depth than 60025 wherein open-system behavior of Sm and Nd was maintained until excavation. Thus, the 370 km represents a minimum diameter for a basin-forming impact that occurred at $4,304 \pm 12$ Ma.

Such a basin-forming impact at ~ 4.30 Ga is not consistent with Late Heavy Bombardment hypothesis in which there was a prolonged increase in impact flux between 3.5 and ~ 4.1 Ga, preceded by a period of relative quiescence from ~ 4.1 to 4.4 Ga (Bottke & Norman, 2017). Several other lunar samples also yield evidence for large impacts in the reputed period of quiescence. These include the coarse-grained impact breccia 67955 which is interpreted to be derived from a basin-forming event at 4.22 ± 0.01 Ga (Norman & Nemchin, 2014). Likewise, the Ar-Ar age of 76535 of 4.23 ± 0.06 Ga has been interpreted by Garrick-Bethell et al. (2008) as recording the time this sample was excavated from 45-km depth by a crater estimated to be at least 780 km in diameter. These authors further claim that the abundance of ~ 4.2 -Ga ages observed in the Apollo 16 and 17 sample suites are consistent with the formation of the South Pole-Aitken basin (Garrick-Bethell et al., 2008). In any case, there appears to be abundant evidence for large impacts occurring on the Moon between 4.2 and 4.3 Ga. The extent to which this requires modifying the current model for the late accretion history of the Moon is largely predicated on how many discrete impact events can be identified in this time interval.

6. Conclusions

Detailed chronologic constraints on lunar crustal formation are hampered by the limited set of available samples. To address this issue, lithic breccias in the Apollo 16 collection were searched to identify additional material for geochronology. Clast 3A from lithic breccia 60016 was identified and characterized. This clast is a noritic anorthosite containing plagioclase and mafic minerals with anorthite contents and Mg#s consistent with those measured in the ferroan anorthosite suite. The sample has a pokiloblastic texture and compositionally homogeneous phases consistent with slow cooling deep in the lunar crust at a rate of $\sim 10^\circ\text{C}/\text{Myr}$. Geothermometry performed on the pyroxenes indicate that the last temperature of equilibrium Clast 3A experienced was between $1,100^\circ\text{C}$ and $1,000^\circ\text{C}$. Extremely fine grained exsolution lamellae present in pyroxenes suggest that the final stage of cooling was very rapid at approximately $0.2^\circ\text{C}/\text{year}$.

The Ar-Ar age of $4,311 \pm 31$ Ma determined on the clast is concordant with the ^{147}Sm - ^{143}Nd age of $4,302 \pm 28$ Ma, as well as with the ^{146}Sm - ^{142}Nd age of $4,297 + 39/-53$ Ma. The weighted average of these ages is $4,304 \pm 12$ Ma and is interpreted to reflect the time at which Clast 3A was exhumed from the deep crust where it was at a temperature of $1,100^\circ\text{C}$ to $1,000^\circ\text{C}$, and well above the estimated Sm-Nd and Ar-Ar closure temperatures. The cooling history of 60016 Clast 3A is similar to that inferred for another noritic anorthosite, 60025. However, a comparison of textures and mineral compositions in 60025 and Clast 3A demonstrate that 60025 was intruded higher in the lunar crust, where it cooled more rapidly. This accounts for the older Sm-Nd age of 60025 of $4,367 \pm 11$ Ma. Both samples have concordant Ar-Ar ages, potentially reflecting excavation from the crust by the same large impact event at $4,304 \pm 12$ Ma. The depth of intrusion of 60025 is estimated by McCallum and O'Brien (1996) to be 21 km requiring a crater of 370 km in diameter to excavate material from such depth. This is a minimal crater size estimate because Clast 3A solidified at a greater depth than 60025. The identification of a basin-forming impact around 4.3 Ga is consistent with chronologic investigations that have suggested another large impact occurred on the Moon near 4.2 Ga (Garrick-Bethell et al., 2008; Hopkins & Mojzsis, 2015; Kelly et al., 2018; Norman & Nemchin, 2014). The occurrence of basin-forming impacts between 4.2 and 4.3 Ga contradicts the reputed period of decreased impact flux inferred to have occurred in the inner solar system between 4.1 and 4.4 Ga prior to the hypothesized uptick in impact flux at ~ 3.8 Ga.

Acknowledgments

Thoughtful and detailed reviews by S. Valencia, S. Mojzsis, R. Burgess, and one anonymous reviewer improved the quality of this work and are appreciated. This work was performed under the auspices of the U.S. Department of Energy by Lawrence Livermore National Laboratory under contract DE-AC52-07NA27344. LLNL-JRNL-759299. This work was supported by NASA Cosmochemistry grants NNH12AT84I and NNH16AC441 (L.E.B.) and Laboratory Directed Research and Development grant 17-ERD-001 (L.E.B.) and NASA Cosmochemistry grant NNX10AI77G to C.K.S. All data associated with this manuscript are available in the supporting information associated with this contribution.

References

- Alibert, C., Norman, M. D., & McCulloch, M. T. (1994). An ancient age for a ferroan anorthosite clast from lunar breccia 67016. *Geochimica et Cosmochimica Acta*, *58*(13), 2921–2926. [https://doi.org/10.1016/0016-7037\(94\)90125-2](https://doi.org/10.1016/0016-7037(94)90125-2)
- Anders, E., Massey, H. S. W., Brown, G. M., Eglinton, G., Runcorn, S. K., & Urey, H. C. (1977). Chemical compositions of the Moon, Earth, and eucrite parent body. *Philosophical Transactions of the Royal Society A*, *285*(1327), 23–40. <https://doi.org/10.1098/rsta.1977.0040>
- Arvidson, R., Crozaz, G., Drozd, R. J., Hohenberg, C. M., & Morgan, C. J. (1975). Cosmic ray exposure ages of features and events at the Apollo landing sites. *The Moon*, *13*(1–3), 259–276. <https://doi.org/10.1007/BF00567518>
- Bohlen, S. R., & Essene, E. J. (1978). Igneous pyroxenes from metamorphosed anorthosite massifs. *Contributions to Mineralogy and Petrology*, *65*(4), 433–442. <https://doi.org/10.1007/BF00372290>
- Borg, L. E., Connelly, J. N., Boyet, M., & Carlson, R. W. (2011). Evidence that the Moon is either young or did not have a global magma ocean. *Nature*, *477*(7362), 70–72. <https://doi.org/10.1038/nature10328>
- Borg, L. E., Connelly, J. N., Cassata, W., Gaffney, A. M., & Bizzarro, M. (2017). Chronologic implications for slow cooling of troctolite 76535 and temporal relationships between the Mg-suite and the ferroan anorthosite suite. *Geochimica et Cosmochimica Acta*, *201*, 377–391. <https://doi.org/10.1016/j.gca.2016.11.021>
- Borg, L. E., Gaffney, A. M., Kruijer, T. S., Marks, N. A., Sio, C. K., & Wimpenny, J. (2019). Isotopic evidence for a young lunar magma ocean. *Earth and Planetary Science Letters*, *523*, 115706. <https://doi.org/10.1016/j.epsl.2019.07.008>
- Borg, L. E., Gaffney, A. M., & Shearer, C. K. (2015). A review of lunar chronology revealing a preponderance of 4.34–4.37 Ga ages. *Meteoritics & Planetary Science*, *50*(4), 715–732. <https://doi.org/10.1111/maps.12373>
- Borg, L. E., Norman, M. D., Nyquist, L. E., Bogard, D., Snyder, G. A., Taylor, L. A., & Lindstrom, M. (1999). Isotopic studies of ferroan anorthosite 62236: A young lunar crustal rock from a light rare-earth element-depleted source. *Geochimica et Cosmochimica Acta*, *63*(17), 2679–2691. [https://doi.org/10.1016/S0016-7037\(99\)00130-1](https://doi.org/10.1016/S0016-7037(99)00130-1)
- Bottke, W. F., & Norman, M. D. (2017). The late heavy bombardment. *Annual Review of Earth and Planetary Sciences*, *45*(1), 619–647. <https://doi.org/10.1146/annurev-earth-063016-020131>
- Boyet, M., & Carlson, R. W. (2007). A highly depleted moon or a non-magma ocean origin for the lunar crust? *Earth and Planetary Science Letters*, *262*(3–4), 505–516. <https://doi.org/10.1016/j.epsl.2007.08.009>
- Brandon, A. D., Lapen, T. J., Debaille, V., Beard, B. L., Rakenburg, K., & Neal, C. R. (2009). Re-evaluating $^{142}\text{Nd}/^{144}\text{Nd}$ in lunar mare basalts with implications for the early evolution and bulk Sm/Nd of the Moon. *Geochimica et Cosmochimica Acta*, *73*(20), 6421–6445. <https://doi.org/10.1016/j.gca.2009.07.015>
- Cadogan, P. H., & Turner, G. (1977). ^{40}Ar - ^{39}Ar dating of Luna 16 and Luna 20 samples. *Philosophical Transactions of the Royal Society of London A*, *284*(1319), 167–177. <https://doi.org/10.1098/rsta.1977.0007>

- Carlson, R. W., Borg, L. E., Gaffney, A. M., & Boyet, M. (2014). Rb-Sr, Sm-Nd and Lu-Hf isotope systematics of the lunar Mg-suite: The age of the lunar crust and its relation to the time of Moon formation. *Philosophical Transactions of the Royal Society of London A*, *372*(2024), 20130246. <https://doi.org/10.1098/rsta.2013.0246>
- Carlson, R. W., & Lugmair, G. W. (1988). The age of ferroan anorthosite 60025: Oldest crust on a young Moon? *Earth and Planetary Science Letters*, *90*(2), 119–130. [https://doi.org/10.1016/0012-821X\(88\)90095-7](https://doi.org/10.1016/0012-821X(88)90095-7)
- Cassata, W. S., & Borg, L. E. (2016). A new approach to cosmogenic corrections in $^{40}\text{Ar}/^{39}\text{Ar}$ chronometry: Implications for the ages of Martian meteorites. *Geochimica et Cosmochimica Acta*, *187*, 279–293.
- Cassata, W. S., & Renne, P. R. (2013). Systematic variations of argon diffusion in feldspars and implications for thermochronometry. *Geochimica et Cosmochimica Acta*, *112*, 251–287. <https://doi.org/10.1016/j.gca.2013.02.030>
- Cherniak, D. J. (2003). REE diffusion in feldspar. *Chemical Geology*, *193*(1–2), 25–41. [https://doi.org/10.1016/S0009-2541\(02\)00246-2](https://doi.org/10.1016/S0009-2541(02)00246-2)
- Cherniak, D. J., & Liang, Y. (2007). Rare earth element diffusion in natural enstatite. *Geochimica et Cosmochimica Acta*, *71*(5), 1324–1340. <https://doi.org/10.1016/j.gca.2006.12.001>
- Cohen, B. A., Snyder, G. A., Hall, C. M., Taylor, L. A., & Nazarov, M. A. (2001). Argon-40-argon-39 chronology and petrogenesis along the eastern limb of the Moon from Luna 16, 20 and 24 samples. *Meteoritics and Planetary Science*, *36*(10), 1345–1366. <https://doi.org/10.1111/j.1945-5100.2001.tb01829.x>
- Connelly, J. N., Amelin, Y., Krot, A. N., & Bizzarro, M. (2008). Chronology of the solar system's oldest solids. *The Astrophysical Journal Letters*, *675*(2), L121.
- Edmunson, J., Borg, L. E., Nyquist, L. E., & Asmerom, Y. (2009). A combined Sm–Nd, Rb–Sr, and U–Pb isotopic study of Mg-suite norite 78238: Further evidence for early differentiation of the Moon. *Geochimica et Cosmochimica Acta*, *73*(2), 514–527. <https://doi.org/10.1016/j.gca.2008.10.021>
- Elardo, S. M., McCubbin, F. M., & Shearer, C. K. (2012). Chromite symplectites in Mg-suite troctolite 76535 as evidence for infiltration metasomatism of a lunar layered intrusion. *Geochimica et Cosmochimica Acta*, *87*, 154–177. <https://doi.org/10.1016/j.gca.2012.03.030>
- Elkins-Tanton, L. T., Burgess, S., & Yin, Q.-Z. (2011). The lunar magma ocean: Reconciling the solidification process with lunar petrology and geochronology. *Earth and Planetary Science Letters*, *304*(3–4), 326–336. <https://doi.org/10.1016/j.epsl.2011.02.004>
- Fernandes, V. A., Fritz, J., Weiss, B. P., Garrick-Bethell, I., & Shuster, D. L. (2013). The bombardment history of the Moon as recorded by ^{40}Ar - ^{39}Ar chronology. *Meteoritics and Planetary Science*, *48*(2), 241–269. <https://doi.org/10.1111/maps.12054>
- Ford, C. E., O'Hara, M. J., & Spencer, P. M. (1977). The origin of lunar feldspathic liquids. *Philosophical Transactions of the Royal Society of London A*, *285*(1327), 193–197. <https://doi.org/10.1098/rsta.1977.0055>
- Gaffney, A. M., & Borg, L. E. (2014). A young solidification age for the lunar magma ocean. *Geochimica et Cosmochimica Acta*, *140*, 227–240. <https://doi.org/10.1016/j.gca.2014.05.028>
- Ganguly, J., & Tirone, M. (1999). Diffusion closure temperature and age of a mineral with arbitrary extent of diffusion: Theoretical formulation and applications. *Earth and Planetary Science Letters*, *170*(1–2), 131–140. [https://doi.org/10.1016/S0012-821X\(99\)00089-8](https://doi.org/10.1016/S0012-821X(99)00089-8)
- Garrick-Bethell, I., Fernandes, V. A., Weiss, B. P., Shuster, D. L., & Becker, T. A., (2008). 4.2 billion year old ages from Apollo 16, 17, and the lunar farside: Age of the South Pole-Aitken Basin? *Workshop on the Early Solar System Impact Bombardment, held November 19–20, 2008 in Houston, Texas*, LPI Contribution No. 1439., pp. 34–35.
- Haskin, L. A., Korotev, R. L., Gillis, J. J., & Jolliff, B. L., (2002). Stratigraphies of Apollo and Luna highland landing sites and provenances of materials from the perspective of basin impact ejecta modeling. *33rd Lunar Planetary Science Conference Abstract*, 1364.
- Herbert, F., Drake, M. J., Sonett, C. P., & Wiskerchen, M. J. (1977). Some constraints on the thermal history of the lunar magma ocean. In *Lunar Science Conference Proceedings*, (Vol. 8, pp. 573–582). New York: Pergamon Press, Inc.
- Hess, P. C., & Parmentier, E. M. (1995). A model for the thermal and chemical evolution of the Moon's interior: Implications for the onset of mare volcanism. *Earth and Planetary Science Letters*, *134*(3–4), 501–514. [https://doi.org/10.1016/0012-821X\(95\)00138-3](https://doi.org/10.1016/0012-821X(95)00138-3)
- Hodges, F. N., & Kushiro, I., (1973). Petrology of Apollo 16 lunar highland rocks. In: *Lunar Science Conference Proceedings*, 4, 1033–1048.
- Hopkins, M. D., & Mojzsis, S. J. (2015). A protracted timeline for lunar bombardment from mineral chemistry, Ti thermometry and U-Pb geochronology of Apollo 14 melt breccia zircons. *Contributions to Mineralogy and Petrology*, *169*(3), 30. <https://doi.org/10.1007/s00410-015-1123-x>
- James, O. B., Lindstrom, M. M., & McGee, J. J., (1991). Lunar ferroan anorthosite 60025: Petrology and chemistry of mafic lithologies. In: *Lunar and Planetary Science Conference Proceedings*, 21, 63–87.
- Kelly, N. M., Flowers, R. M., Metcalf, J. R., & Mojzsis, S. J. (2018). Late accretion to the Moon recorded in zircon (U–Th)/He thermochronometry. *Earth and Planetary Science Letters*, *482*, 222–235. <https://doi.org/10.1016/j.epsl.2017.11.009>
- Kruijjer, T. S., & Kleine, T. (2017). Tungsten isotopes and the origin of the Moon. *Earth and Planetary Science Letters*, *475*, 15–24. <https://doi.org/10.1016/j.epsl.2017.07.021>
- Levine, J., Renne, P. R., & Muller, R. A. (2007). Solar and cosmogenic argon in dated lunar impact spherules. *Geochimica et Cosmochimica Acta*, *71*(6), 1624–1635. <https://doi.org/10.1016/j.gca.2006.11.034>
- Lindsley, D. H. (1983). Pyroxene thermometry. *American Mineralogist*, *68*(5–6), 477–493.
- Lindsley, D. H., & Andersen, D. J. (1983). A two-pyroxene thermometer. *Journal of Geophysical Research*, *88*(S02), A887–A906. <https://doi.org/10.1029/JB088iS02p0A887>
- Ludwig, K. R., (1991). ISOPLOT: A plotting and regressions program for radiogenic isotope data, version 2.53. *USGS Open-file Report 91-0445*. <https://doi.org/10.3133/ofr91445>
- Marks, N. E., Borg, L. E., Hutcheon, I. D., Jacobsen, B., & Clayton, R. N. (2014). Samarium–neodymium chronology and rubidium–strontium systematics of an Allende calcium–aluminum-rich inclusion with implications for ^{146}Sm half-life. *Earth and Planetary Science Letters*, *405*, 15–24. <https://doi.org/10.1016/j.epsl.2014.08.017>
- Martinez, R. R., (1985). Description of sawed surfaces of fragmental polymict breccia 60016, 16. *Curatorial Lunar Newsletter- No. 43*, Appendix 1, 10–22. Lunar Sample Curator, NASA Johnson Space Center, Houston, TX.
- McCallum, I. S., & O'Brien, H. E. (1996). Stratigraphy of the lunar highland crust: Depths of burial of lunar samples from cooling-rate studies. *American Mineralogist*, *81*(9–10), 1166–1175. <https://doi.org/10.2138/am-1996-9-1015>
- McCallum, I. S., & Schwartz, J. M. (2001). Lunar Mg suite: Thermobarometry and petrogenesis of parent magmas. *Journal of Geophysical Research*, *106*(E11), 27,969–27,983. <https://doi.org/10.1029/2000JE001397>
- McKay, D. S., Bogard, D. D., Morris, R. V., Korotev, R. L., Johnson, P., & Wentworth, S. J. (1986). Apollo 16 regolith breccias: Characterization and evidence for early formation in the mega-regolith. *Journal of Geophysical Research*, *91*(B4), 277–303. <https://doi.org/10.1029/JB091iB04p0D277>
- McLeod, C. L., Brandon, A. D., & Armitage, R. M. G. (2014). Constraints on the formation age and evolution of the Moon from ^{142}Nd - ^{143}Nd systematics of Apollo 12 basalts. *Earth and Planetary Science Letters*, *396*, 179–189. <https://doi.org/10.1016/j.epsl.2014.04.007>

- Meissner, F., Schmidt-Ott, W.-D., & Ziegeler, L. (1987). Half-life and α -ray energy of ^{146}Sm . *Zeitschrift für Physik A-Atomic Nuclei*, 327(2), 171–174. <https://doi.org/10.1007/BF01292406>
- Meyer, J., Elkins-Tanton, L., & Wisdom, J. (2010). Coupled thermal–orbital evolution of the early Moon. *Icarus*, 208(1), 1–10. <https://doi.org/10.1016/j.icarus.2010.01.029>
- Nemchin, A. A., Pidgeon, R. T., Whitehouse, M. J., Vaughan, J. P., & Meyer, C. (2008). SIMS U-Pb study of zircon from Apollo 14 and 17 Breccias: Implications for the evolution of lunar KREEP. *Geochimica et Cosmochimica Acta*, 72(2), 668–689. <https://doi.org/10.1016/j.gca.2007.11.009>
- Nord Jr., G.L., (1976). 76535:Thermal history deduced from pyroxene precipitation in anorthite. In: *Proceedings of the Lunar Science Conference 7th*, 2(A77-34651 15-91), 1875–1888.
- Norman, M. D., Borg, L. E., Nyquist, L. E., & Bogard, D. D. (2003). Chronology, geochemistry, and petrology of a ferroan noritic anorthosite clast from Descartes breccia 67215: Clues to the age, origin, structure, and impact history of the lunar crust. *Meteoritics & Planetary Science*, 38(4), 645–661. <https://doi.org/10.1111/j.1945-5100.2003.tb00031.x>
- Norman, M. D., & Nemchin, A. A. (2014). A 4.2 billion year old impact basin on the Moon: U-Pb dating of zirconolite and apatite in lunar melt rock 67955. *Earth and Planetary Science Letters*, 388, 387–398. <https://doi.org/10.1016/j.epsl.2013.11.040>
- Nyquist, L. E., Wiesmann, H., Bansal, B. M., Shih, C.-Y., Keith, J. E., & Harper, C. L. (1995). ^{146}Sm – ^{142}Nd formation interval for the lunar mantle. *Geochimica et Cosmochimica Acta*, 59(13), 2817–2837. [https://doi.org/10.1016/0016-7037\(95\)00175-Y](https://doi.org/10.1016/0016-7037(95)00175-Y)
- Papike, J. J., Fowler, G. W., & Shearer, C. K. (1997). Evolution of the lunar crust: SIMS study of plagioclase from ferroan anorthosites. *Geochimica et Cosmochimica Acta*, 61(11), 2343–2350. [https://doi.org/10.1016/S0016-7037\(97\)00086-0](https://doi.org/10.1016/S0016-7037(97)00086-0)
- Papike, J. J., Ryder, G., & Shearer, C. K. (1998). Chapter 5: Lunar samples. In *Planetary Materials, Reviews in Mineralogy* (Vol. 36, Chap. 5: 1–189.). Washington, DC: Mineralogical Society of America.
- Petro, N. E., & Pieters, C. M. (2006). Modeling the provenance of the Apollo 16 regolith. *Journal of Geophysical Research*, 111, E09005. <https://doi.org/10.1029/2005JE002559>
- Rankenburg, K., Brandon, A. D., & Neal, C. R. (2006). Neodymium isotope evidence for chondritic composition of the Moon. *Science*, 312(5778), 1369–1372. <https://doi.org/10.1126/science.1126114>
- Renne, P. R., Balco, G., Ludwig, K. R., Mundil, R., & Min, K. (2011). Response to the comment by W.H. Schwarz et al. on “Joint determination of ^{40}K decay constants and $^{40}\text{Ar}^*/^{40}\text{K}$ for the Fish Canyon sanidine standard, and improved accuracy for $^{40}\text{Ar}^*/^{39}\text{Ar}$ geochronology” by P.R. Renne et al. (2010). *Geochimica et Cosmochimica Acta*, 75(17), 5097–5100. <https://doi.org/10.1016/j.gca.2011.06.021>
- Renne, P. R., Knight, K. B., Nomade, S., Leung, K.-N., & Lou, T.-P. (2005). Application of deuterium–deuterium (D–D) fusion neutrons to $^{40}\text{Ar}^*/^{39}\text{Ar}$ geochronology. *Applied Radiation and Isotopes*, 62(1), 25–32. <https://doi.org/10.1016/j.apradiso.2004.06.004>
- Ross, M., & Huebner, J.S., (1975). A pyroxene geothermometer based on composition-temperature relationships of naturally occurring orthopyroxene, pigeonite, and augite. *Extended Abstracts of the International Conference of Geothermometry and Geobarometry, Pennsylvania State University, University Park, Pennsylvania*.
- Ross, M., Huebner, J. S., & Dowty, E. (1973). Delineation of the one atmosphere augite-pigeonite miscibility gap for pyroxenes from lunar basalt 12021. *American Mineralogist*, 58(7-8), 619–635.
- Ryder, G. (1990). Lunar samples, lunar accretion and the early bombardment of the Moon. *Eos, Transactions American Geophysical Union*, 71(10), 313–323. <https://doi.org/10.1029/90EO00086>
- Ryder, G. (2002). Mass flux in the ancient Earth-Moon system and benign implications for the origin of life on Earth. *Journal of Geophysical Research*, 107(E4), 5022. <https://doi.org/10.1029/2001JE001583>
- Ryder, G. & Norman, M.D., (1980). Catalog of Apollo 16 rocks, *Apollo 16 Lunar Sample Information Catalog Part I: 60015–62315*, NASA Johnson Space Center Curatorial Branch Publication JSC-16904. Houston, Texas, pp. 1113.
- Shearer, C. K., Burger, P. V., Neal, C., Sharp, Z., Spivak-Birndorf, L., Borg, L., et al. (2010). Non-basaltic asteroidal magmatism during the earliest stages of solar system evolution; a view from Antarctic achondrites Graves Nunatak 06128 and 06129. *Geochimica et Cosmochimica Acta*, 74(3), 1172–1199. <https://doi.org/10.1016/j.gca.2009.10.029>
- Shearer, C. K., Burger, P. V., Papike, J. J., Borg, L. E., Irving, A. J., & Herd, C. (2008). Petrogenetic linkages among Martian basalts: Implications based on trace element chemistry of olivine. *Meteoritics & Planetary Science*, 43(7), 1241–1258. <https://doi.org/10.1111/j.1945-5100.2008.tb01126.x>
- Shearer, C. K., Elardo, S. M., Petro, N. E., Borg, L. E., & McCubbin, F. M. (2015). Origin of the lunar highlands Mg-suite: An integrated petrology, geochemistry, chronology, and remote sensing perspective. *American Mineralogist*, 100(1), 294–325. <https://doi.org/10.2138/am-2015-4817>
- Shearer, C. K., Hess, P. C., Wiczorek, M. A., Pritchard, M. E., Parmentier, M. E., Borg, L. E., et al. (2006). Thermal and magmatic evolution of the Moon. In B. L. Jolliff, M. A. Wiczorek, C. K. Shearer, & C. R. Neal (Eds.), *New views of the Moon*, Reviews in Mineralogy and Geochemistry, (Vol. 60, pp. 365–518). <https://doi.org/10.2138/rmg.2006.60.4>
- Shearer, C. K., & Papike, J. J. (2005). Early crustal building processes on the Moon: Models for the petrogenesis of the magnesium suite. *Geochimica et Cosmochimica Acta*, 69(13), 3445–3461. <https://doi.org/10.1016/j.gca.2005.02.025>
- Shuster, D. L., & Cassata, W. S. (2015). Paleotemperatures at the lunar surfaces from open system behavior of cosmogenic ^{38}Ar and radiogenic ^{40}Ar . *Geochimica et Cosmochimica Acta*, 155, 154–171. <https://doi.org/10.1016/j.gca.2015.01.037>
- Sio, C.K. & Borg, L.E., (2018). Sm-Nd isotopic systematics of ferroan anorthosite (FAN) 62237: Evidence for co-magmatism of FANs at 4.36 Ga. *Proceedings of the 49th Lunar and Planetary Science Conference*, Abstr. #2083.
- Snyder, G. A., Taylor, L. A., & Neal, C. R. (1992). A chemical model for generating the source of mare basalts: Combined equilibrium and fractional crystallization of the lunar magmashpere. *Geochimica et Cosmochimica Acta*, 56(10), 3809–3823. [https://doi.org/10.1016/0016-7037\(92\)90172-F](https://doi.org/10.1016/0016-7037(92)90172-F)
- Solomon, S.C., & Longhi, J., (1977). Magma oceanography: 1. Thermal evolution. In: *Abstracts of the Lunar and Planetary Science Conference*. 8, pp. 884.
- Stewart, D.B., (1975). Apollonian metamorphic rocks—The products of prolonged subsolidus equilibration. *Abstracts of the Lunar and Planetary Science Conference*, 6, 774–776.
- Tanaka, T., Togashi, S., Kamioka, H., Amakawa, H., Kagami, H., Hamamoto, T., et al. (2000). JNdi-1: A neodymium isotopic reference in consistency with LaJolla neodymium. *Chemical Geology*, 168(3-4), 279–281. [https://doi.org/10.1016/S0009-2541\(00\)00198-4](https://doi.org/10.1016/S0009-2541(00)00198-4)
- Taylor, S.R., (1982). Planetary science: A lunar perspective, Lunar and Planetary Institute, Houston, Texas, pp. 481
- Van Orman, J. A., & Grove, T. L. (2000). Origin of lunar high-titanium ultramafic glasses: Constraints from phase relations and dissolution kinetics of clinopyroxene-ilmenite cumulates. *Meteoritics & Planetary Science*, 35(4), 783–794. <https://doi.org/10.1111/j.1945-5100.2000.tb01462.x>

- Wänke, H., Palme, H., Baddenhausen, H., Dreibus, G., Kruse, H., & Spettel, B. (1977). Element correlations and the bulk composition of the Moon. *Philosophical Transactions of the Royal Society A*, *285*(1327), 41–48. <https://doi.org/10.1098/rsta.1977.0041>
- Warren, P. H., & Wasson, J. T. (1979). The origin of KREEP. *Reviews of Geophysics*, *17*(1), 73–88. <https://doi.org/10.1029/RG017i001p00073>
- Wieczorek, M. A., & Phillips, R. J. (1999). Lunar multiring basins and the cratering process. *Icarus*, *139*(2), 246–259. <https://doi.org/10.1006/icar.1999.6102>
- Wieler, R. (2002). Cosmic-ray-produced noble gases in meteorites. *Reviews in Mineralogy and Geochemistry*, *47*(1), 125–170. <https://doi.org/10.2138/rmg.2002.47.5>
- Wood, J. A., Dickey, J. S., Marvin, U. B., & Powell, B. N. (1970). Lunar anorthosites. *Science*, *167*(3918), 602–604. <https://doi.org/10.1126/science.167.3918.602>